Metal−Molecule Schottky Junction Effects in Surface Enhanced Raman Scattering

Manas Ranjan Gartia,[†,§] Tiziana C. Bond,[‡] and Gang Logan Liu*[,§]

Department of Nuclear, Plasma and Radiological Engineering, University of Illinois, Urbana−Champaign, Illinois 61801, United States, Meso, Micro and Nano Technologies Center, Lawrence Livermore National Laboratory, 7000 East Avenue, Livermore, California 94550, United States, and Micro and Nanotechnology Laboratory, Department of Electrical and Computer Engineering, University of Illinois, Urbana−Champaign, Illinois 61801, United States

Received: July 14, 2010; Revised Manuscript Received: November 15, 2010

We propose a complementary interpretation of the mechanism responsible for the strong enhancement observed in surface enhanced raman scattering (SERS). The effect of a strong static local electric field due to the Schottky barrier at the metal−molecule junction on SERS is systematically investigated. The study provides a viable explanation to the low repeatability of SERS experiments as well as the Raman peak shifts as observed in SERS and raw Raman spectra. It was found that a strong electrostatic built-in field at the metal-molecule junction along specific orientations can result in 2−4 more orders of enhancement in SERS.

Introduction

Since its discovery,[1−3] surface enhanced raman scattering (SERS) is progressively breaking new grounds and now even applied for the detection of more complex molecules and biologically relevant materials.[4] The single molecule detection capability[5,6] has enhanced the prospect of using Raman probe in sensor application,[7−9] hazardous materials detection,[10,11] and more recently, probing biological structures.[12,13] Over the years three possible mechanisms for enhancement in Raman scattering have been identified:[14] (i) the surface plasmon resonance in the metal particle (or electromagnetic mechanism),[2,3,15−19] (ii) a charge transfer resonance involving transfer of electrons between the molecule and metal energy level (or simply charge transfer mechanism),[16,20−27] (iii) resonance within the molecule itself.[14] The well-known electromagnetic (EM) mechanism can be described as follows: when the incident laser frequency (or wavelength) is in resonance with the plasmon mode of the nanoparticle, a large amount of energy can be "concentrated" by the nanoparticle.[28] Subsequently, the nanoparticle re-emits a portion of the EM energy by Mie scattering, thereby creating an intense surface field with very high energy density at or near the particle surface. In general, EM enhancement should amplify the Raman scattering nonselectively irrespective of type of molecules adsorbed on a particular surface.[29] However, the molecules CO and N_2 differ by a factor of 200 in their SERS intensities under the same experimental conditions.[26] Another interesting example is that of water. While many SERS studies are conducted in aqueous systems, there is rarely an enhancement in the Raman spectrum of water. These results cannot be explained by invoking only electromagnetic enhancement. Further, when the coupling of chemical enhancement effect of the nanoparticles is considered, the EM enhancement of SERS can be up to the order of 10^{10}.[30] The huge enhancement factor ($10^{14}-10^{15}$) as seen in many single-molecule experiments are normally attributed to the low concentration level of the analyte in SERS experiments and hence, mainly due to the difference in the number of molecules showing scattering in SERS as compared to bulk Raman.[31] However, the contribution from electromagnetic coupling and chemical binding are clearly inseparable in experiments due to the fact that the SERS detection itself depends on the electromagnetic enhancement process.[32] Thus the kind of charge transfer (CT) contribution in those high enhancement experiments ($10^{14}-10^{15}$) is still unknown. In the charge transfer model,[33] an incident photon excites an electron from the metal surface into an adsorbed molecule, creating a negatively charged excited molecule. The molecular geometry of this excited molecule differs from that of the neutral species. This charge transfer induces a nuclear relaxation within the excited molecule, which results in the return of the electron to the metal surface, the creation of an excited neutral molecule, and the emission of a wavelength shifted (Raman) photon.[18] In principle, in the CT an adsorbed molecule can, under specific conditions, interact with a metal surface in such a way that there is a large increase in molecular polarizability (change), α. Further, it was shown experimentally that the charge transfer can occur in both directions (that is, metal cluster-to-molecule or molecule-to-metal cluster) depending on the relative energies of the metal Fermi level and the HOMO (highest occupied molecular orbital) and LUMO (lowest unoccupied molecular orbital) levels of the adsorbed molecule.[22] For example, molecules with low-lying unfilled π-orbitals (such as pyridine) experienced metal-to-molecule transfer, while those without low-lying unfilled orbitals (such as NH_3 or piperidine) tended to transfer electrons to the metal.[14,22]

It is also important to realize that the aforementioned three mechanisms are not independent of each other, but rather the total enhancement is due to the result of combine effect of one or more of the three mechanisms depending on the wavelength used in the experiment and the specific adsorbate and metal.[34] Even though it may not always be possible to separate these different mechanisms experimentally or theoretically, certain limits can be established where one mechanism is more dominating than the others. In fact, to isolate the CT enhance-

* Corresponding authors. E-mail: G.L.L., loganliu@illinois.edu; T.C.B., bond7@llnl.gov.
† Department of Nuclear, Plasma and Radiological Engineering, University of Illinois.
§ Micro and Nanotechnology Laboratory, Department of Electrical and Computer Engineering, University of Illinois.
‡ Lawrence Livermore National Laboratory.

10.1021/jp1065083
Published on Web 12/28/2010

ment, SERS has been studied for adsorbates on smooth surfaces, which are known to be incapable of supporting large surface plasmons. These studies showed only small (10^1-10^2) enhancements.[35,36] However, recent theoretical[37] as well as experimental[38,39] studies has shown that under certain conditions the CT enhancement can be much larger than is usually predicted earlier. In addition, large SERS enhancements have also been observed for molecules interacting with small nanoclusters or nanocrystalline semiconductor surfaces, both of which are not expected to support plasmon resonances and thus should show only small EM enhancement.[40−42] However, the CT mechanism has been widely studied and fairly gives an intuitive picture of the chemical enhancement, it mostly relies on phenomenological parameters.[16,24] In this context, it is increasingly important to understand the microscopic nature of SERS using first principle modeling.[43] It is now widely believed that the chemical bonding effects in SERS can be simulated just by considering the local environment of a molecule, which is also consistent with the adatom model.[26,44] The adatom model assumes that the atomic-scale roughness features determine the hot spots on a metal surface and invariably discount the electromagnetic enhancement due to the excitation of surface plasmons in the metal as well as the effect of interference between the chemical and the electromagnetic mechanism if any. Indeed, in such an approach the CT and EM effects enter in multiplicative fashion in the total enhancement factor.[45] Also, in most of the previous theoretical studies of SERS, only a few metal atoms were used to model the molecule/surface interaction. For example, Aroca et al.[46] did the simulation with just a single silver atom to mimic the chemisorption of phthalimide on a silver surface and obtained a reasonable agreement with experiments. Similarly, resonance Raman calculation,[47] SERS study of pyridine adsorbed on silver clusters,[34,37,48] and SERS simulation for benzenethiol adsorbed on Ag surface[44] have been performed with fair success by using a few tens of atoms. It has also been shown by using rigorous density functional theory (DFT) computation by using large surface unit cells that the ($\sqrt{3} \times \sqrt{3}$) unit cell is sufficient to treat the single molecule adsorption of benzenethiol on Au (111) surface in the low coverage limit.[49] A full coverage can be defined as one thiol molecule per three Au surface atoms, which is consistent with our simulation approach. The STM experiments for structure of benzenethiol adsorbed on gold (111) showed surface coverage of about 0.306 for the benzenethiol molecule.[50] In this paper, simulations for chemical bonding effects on Raman scattering have been performed for benzenethiol using 1−3 gold atoms.

The various issues considered so far in the context of chemical enhancement includes the binding geometry of the adsorbate,[51] the effects of adsorption on various noble and transition metal surfaces,[52] the influence of positively charged atoms at the metal surface,[53,54] the effect of adsorbed chloride anions,[55] the effect of nonzero static electric fields,[56] and the solvent effects in the calculations.[57] Although there is clear evidence of the existence of a solid−liquid electrochemical interface (electric double layer) in all aqueous SERS experiment as well as metal−molecule interface in nonaqueous SERS experiments, there is no systematic study so far to elucidates these effects. It is also well-known that the strong electric field present at such an interface perturbs the vibrational frequencies of the adsorbed species, the vibrational Stark effect (VSE).[1,58] In addition, the electric field also changes the adsorbate vibrational line strength, the vibrational intensity effect (VIE).[59,60] Here we present a systematic study of both of these effects on a model SERS molecule, benzenethiol, by assuming an interfacial static electric field between metal−molecule interface whose magnitude and direction are taken as parameters of the model. The external static electric field can be seen as a perturbation to the system Hamiltonian. Our present computational approach is also motivated by the goal of interpretation of potential dependent SERS studies.[61,62] In a recent experiment, an enhancement on the order of 10^5-10^9 was observed upon application of external electric field to glutamic acid adsorbed on a Ag substrate.[63] The present study aims to provide a microscopic insight to any such studies and may lead to achieving applied electric field controllable SERS intensity module. To present a simplified picture of the metal−molecule interface, the molecule has been considered as a semiconductor (the justification is described below) and the magnitude of the static electric field so developed is calculated on the basis of the metal−molecule Schottky barrier mechanism.

Molecule as Semiconductor

Most organic materials are electrical insulators with values of electrical conductivity at room temperature in the range $10^{-9}-10^{-14}$ S cm^{-1} [64] (10^9-10^{14} Ω cm resistivity). To obtain a larger conductivity and hence semiconducting behavior, the HOMO−LUMO gap needs to be reduced; this can be achieved with extensive π-bonding. This reduced band gap allows electrons to more easily jump between conduction and valence bands and gives rise to the semiconductive properties.[65] In crystalline semiconductor technologies, n-type and p-type refer to the type of dopant, and therefore majority carrier, in a semiconductor. In crystalline materials both holes and electrons can usually be transported reasonably well. It is, nevertheless, common in the literature to refer to hole transporting disordered (doped) semiconductor materials as p-type and electron transporting materials as n-type because this describes their majority carriers and semiconducting behavior.

On the other hand, aromatic rings contain alternating single and double bonds that lead to overlapping p-orbitals, which form π-bonds. In π-bonds, electrons delocalize and are shared between the atoms on the ring's backbone. Similar to conduction due to a delocalized "sea of electrons" in metals, free movement of delocalized π-electrons in organic compounds allows organic molecules to conduct electricity and behave as semiconductors.[66] Then how to distinguish p-type or n-type organic semiconductor? In view of the popular organic semiconductor field, electron-rich conjugated polymers are termed as p-type and electron-poor ones are termed as n-type.[67] For example, in benzenethiol, the hydrogen atoms which surround the carbon backbone are less electronegative than the carbon backbone itself and lend some electron density to the delocalized π-electron cloud. The electron rich conjugated molecule has difficulty accepting another electron but is able to lose an electron with relative ease. As a consequence, positive charge carriers are expected to dominate transport in benzenethiol molecule.[66] In other words, molecules involving π-conjugation have high HOMO levels and exhibit electron-donating properties. Hence, these molecules are good candidates for p-type semiconductors.[68]

However, it should be recognized here that the view of holes and electrons π-orbital molecule as free carriers is rather simplistic. It allows us to make some general predictions about the trends in energy levels if we use it carefully but may not extend well to all polymers.[66] It should also be recognized that the expected carrier mobility in such organic semiconductor is typically low (~1 cm^2 V^{-1} s^{-1}) as compared to traditional inorganic semiconductors (for silicon crystal ~300−900 cm^2 V^{-1} s^{-1}).

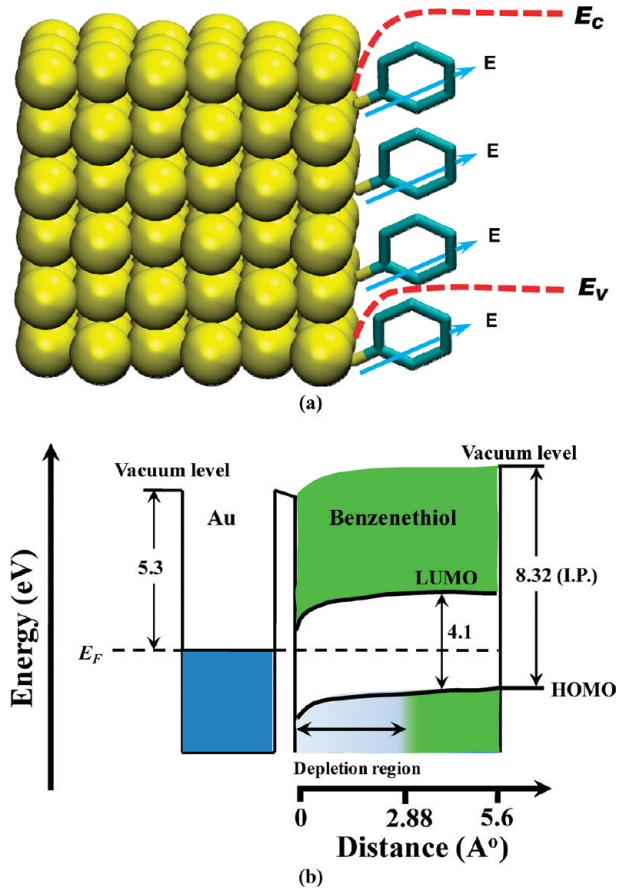

Figure 1. (a) Schematic of metal−molecule Schottky barrier junction, the monolayer of benzenethiol molecules on the gold cluster surface with perpendicular electric field orientation. (b) Schematic energy-band diagram of the gold/benzenethiol Schottky junction interface. E_F is the Fermi energy of metal, and IP is the ionization potential.

Metal−Molecule Interface

It is well-known that a potential barrier known as a Schottky barrier forms at a metal−semiconductor junction[69,70] and the built-in electrostatic field strength can be as high as a few volts per angstrom. The formation of a Schottky barrier between a metal electrode and organic electronics materials has been extensively studied both theoretically[71−73] and experimentally[74−77] in recent years. In addition, the application of SAMs (self-assembled monolayers) of π-conjugated thiols for single-molecule electronics have been extensively studied.[78] Herein we assume the benzenethiol molecule is equivalent to a highly doped p-type semiconductor and the gold−benzenethiol junction is equivalent to a metal−semiconductor Schottky barrier junction, as shown in Figure 1a. Providing a self-assembly monolayer coverage of 6.8×10^{14} cm^{-2} for benzenethiol on the gold surface,[79,80] the packing density of benzenethiol or equivalently the electron donor concentration can be calculated to be $N_D = 1.36 \times 10^{22}$ cm^{-3}. The depletion width at the metal−molecule junction can be calculated using the relation $W = [2\varepsilon_s\phi_s/qN_D]^{1/2}$, where ε_s is the permittivity of benzenethiol molecule, ϕ_s is the surface potential, q is the fundamental electric charge. The maximum surface potential ϕ_s is approximated as half of the energy band gap of the benzenethiol molecule, which is about 2 eV. Taking the relative permittivity (ε_r) of benzenethiol as 4.38[81] the depletion width of our system was thus found to be 2.88 Å. The built-in electric field was calculated using the simple relation $E_0 = (q/\varepsilon)WN_D$ and found to be 1.41 V/Å. It should be noted that this estimated electric field strength is the maximum value and the real built-in electric field should be slightly lower than this value. Figure 1b displays the schematic of the energy-band diagram of a gold/benzenethiol Schottky junction, using the parameters obtained in our analysis. The work function of Au is 5.3 eV,[82] the ionization potential (IP) of benzenethiol is 8.32 eV.[83,84] The band gap of benzenethiol was calculated to be 4.1 eV. The difference between the Fermi energy of the metal and HOMO (highest occupied molecular orbital) is known as HIB (hole injection barrier) and the difference in the Fermi level and that of the LUMO (lowest unoccupied molecular orbital) of the organic molecule is known as EIB (electron injection barrier).[71,77] In the present study HIB is calculated to be ~2.06 eV and EIB is calculated to be ~2.04 eV.

Now, the interface between metal and organic semiconducting layers can be described with the help of screening parameter (S parameter)[85] which is defined as $S = d\phi_B^P/d\phi_m$, where ϕ_m and ϕ_B^Pdenote the work function of the metal and the barrier height for carrier injection at the interface for holes (HIB), respectively. $S = 0$ corresponds to the so-called Bardeen limit for which Fermi level pinning occurs. Similarly, $S = 1$ corresponds to an ideal Schottky barrier at the interface (Schottky limit).[86] For metal−organic molecule interfaces formed by chemical bonds, it is reasonable to interpret the Bardeen limit as the situation where strong orbital interactions between frontier orbitals of metals and the HOMO of a molecule occurs and the Schottky limit as the situations where weak orbital interactions occurs between them. In other words, when molecules have large energy gaps between the HOMO and the LUMO, as in the present study, the Schottky limit holds well.[86] In fact the value of S was calculated to be 0.5 experimentally for Au and benzenethiol system.[86] Again the density of states $D(E_F)$ of interfacial electronic states can be calculated using the relation, $S = (1 + e^2\delta D(E_F)/\varepsilon)^{-1}$,[85−87] where e, δ, and ε denote the elementary charge, width of the metal−molecule interface, and dielectric constant, respectively. Taking δ and ε to be 5.7 and 4.38 Å for benzenethiol[81] respectively, $D(E_F)$ is estimated to be 4.2×10^{13} states/(cm^2·eV), which is less than 20% of the density of states of Au at the Fermi level.[88] Even though small, the existence of a finite density of states for the frontier orbitals of the molecule near the Fermi level indicates that electrons pass through hybrid orbitals composed of frontier orbitals of the metal and molecule supporting the charge transfer mechanism.

Computational Approach and Details

Using a simple model, we have estimated the built-in electric field of the order of few V/Å. The effect of such a high built-in electric field on the molecular conformation and electronic and vibrational properties was probed using a quantum mechanical simulation. The theoretical simulations were performed using density functional theory (DFT) implemented in the Amsterdam density functional (ADF) program package.[89,90] DFT methods are based on the Hohenberg−Kohn theorem, which states that the ground state electronic energy of a molecule can be expressed exactly as the electron density of the molecule. The Becke−Perdew (BP86) XC-potential[91,92] and a triple-ζ polarized slater type (TZP) basis set from the ADF basis set library were used in our simulation. For a metal adsorbed molecule, a frozen core was chosen for Au during the vibrational frequency calculation to reduce the computational time. The zeroth-order regular approximation (ZORA) was employed to account for the scalar relativistic effects. For neat benzenethiol calculation, a large core without relativity and with an integration accuracy of 4.0 was used. The SCF convergence criterion was kept at

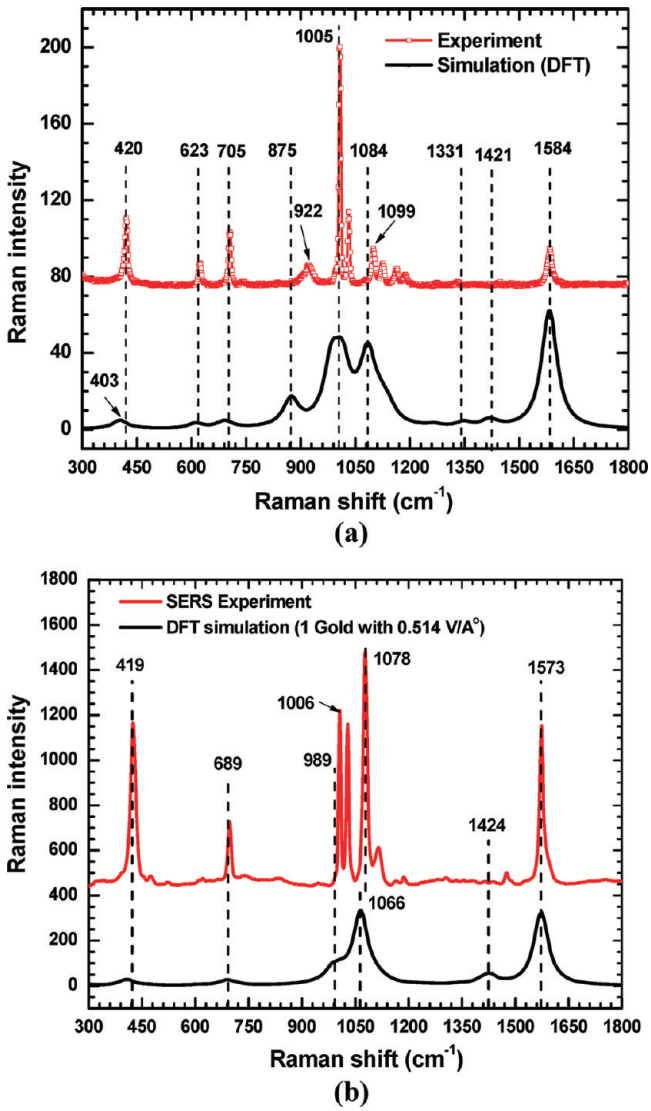

Figure 2. (a) Comparison of results obtained from a DFT study with experiments. The spectra shown are for neat Raman. (b) Comparison of SERS spectra of benzenethiol calculated by DFT simulation and obtained from experiment.

10^{-8}. Frequencies preset were run in the ADF-GUI mode to obtain the Raman frequencies. Automatic electron smearing (in the case of problematic SCF convergence) was disabled. All frequency calculations are run after geometry convergence is achieved. The polarizability derivative and Raman frequencies are calculated internally by the ADF-GUI module (no external numerical calculation was performed). The validity of using DFT and ADF for quantum mechanical SERS calculation has already been proven by many researchers.[37−48] Further, in the present study, the validity of our results has been checked by comparing the computational results for the Raman as well as SERS spectra with the experimental results. The details of the experiments have been given elsewhere.[93] The simulated results match fairly well with the experiments, as shown in Figure 2. Comparison of results obtained from DFT study with experiments for neat Raman is shown in Figure 2a. Similarly, the result for SERS spectra of benzenethiol calculated by DFT simulation and obtained from experiment is shown in Figure 2b. Clearly the characteristics peaks observed in the experiments are captured by the DFT simulation.

Results and Discussion

The polarization effect of SERS has already in observed in single molecule experiment[5] and recently been verified with a computational model.[94] Here, we investigate the effect of built-in electric field direction on the Raman scattering process. To model such a system, first a static electric field is applied on the benzenethiol molecule along various directions to simulate the built-in field of Schottky barrier developed at the metal−molecule junction. The molecular conformation under different conditions is found through the energy minimization process in each case. Here, all the directions are related to the molecular coordinates and hence positive *Z*-direction should be normal to the benzene ring structure. Figure 3a shows the deformation in chemical bond length of benzenethiol molecule due to application of electric fields. In general, it was found that the extent of the bond length change is proportional to the built-in electric field. Depending on the relative orientations between the molecule and the built-in electric field, different trends are shown for the length change of various chemical bonds such as the carbon−sulfur bond and carbon6−sulfur bond. The largest change in bond length and dihedral angle was seen when the built-in field was perpendicular to the benzene ring (positive *Z*-direction). The dihedral bond angle also changes as shown in Figure 3b. One can clearly see that the built-in field leads to a large variation in bond length and dihedral angle at specific orientations. To emphasize the change in bond orientation and length under application of electric field, the actual conformation of benzenethiol molecule is shown as obtained from our simulation in Figure 3c. The molecular conformation change will inherently induce dipole moment and polarizability changes since the interatomic distance and angle are altered (please see the Supporting Information). The direct correlation between the built-in electric field and the polarizability derivative of two dipoles in benzenethiol molecule is shown in Figure 3d. These two dipoles correspond to the vibrational modes at 403 and 1573 cm^{-1}, respectively. The trend in the change of bond length and change in the polarizability is consistent with other theoretical prediction.[37,44]

The close-up of the peaks is also shown in the inset. The large enhancement of a peak in particular direction can be assigned to the largest change in the polarizability derivative in that direction. In the particular case shown here, for example, the largest change in polarizability derivative for 403 cm^{-1} peak is in the $+Z$ direction (perpendicular to benzene ring) and, hence, the largest enhancement one could see for that peak is in the $+Z$ direction. Similarly, for 1573 cm^{-1} peak, the largest change in polarizability derivative observed was in the $+X$ direction (parallel to benzene ring structure). That is why the largest enhanced 1573 cm^{-1} peak corresponds to electric field applied in the $+X$ direction. For a similar molecule, pyridine, Arenas et al.[95] found experimentally that the modes at 410, 598, 1204, and 1573 cm^{-1} show the strongest dependence on the electrode potential. The theoretical TDDFT simulation for benzenethiol adsorbed on silver cluster shows a similar trend,[44] which is in agreement with current simulation results.

The graphical explanation for the effect of a built-in field at the Schottky barrier on the molecular dipole moment is shown in Figure 4. The molecular quantum states can be described on the basis of the Born−Oppenheimer separation of nuclear and electronic degrees of freedom. The electrons are much lighter than nuclei and can adjust rapidly to the instantaneous nuclear configuration (which is also known as the Franck−Condon principle). Therefore, molecules are characterized by "potential energy surfaces" (plots of energy versus internuclear separation)

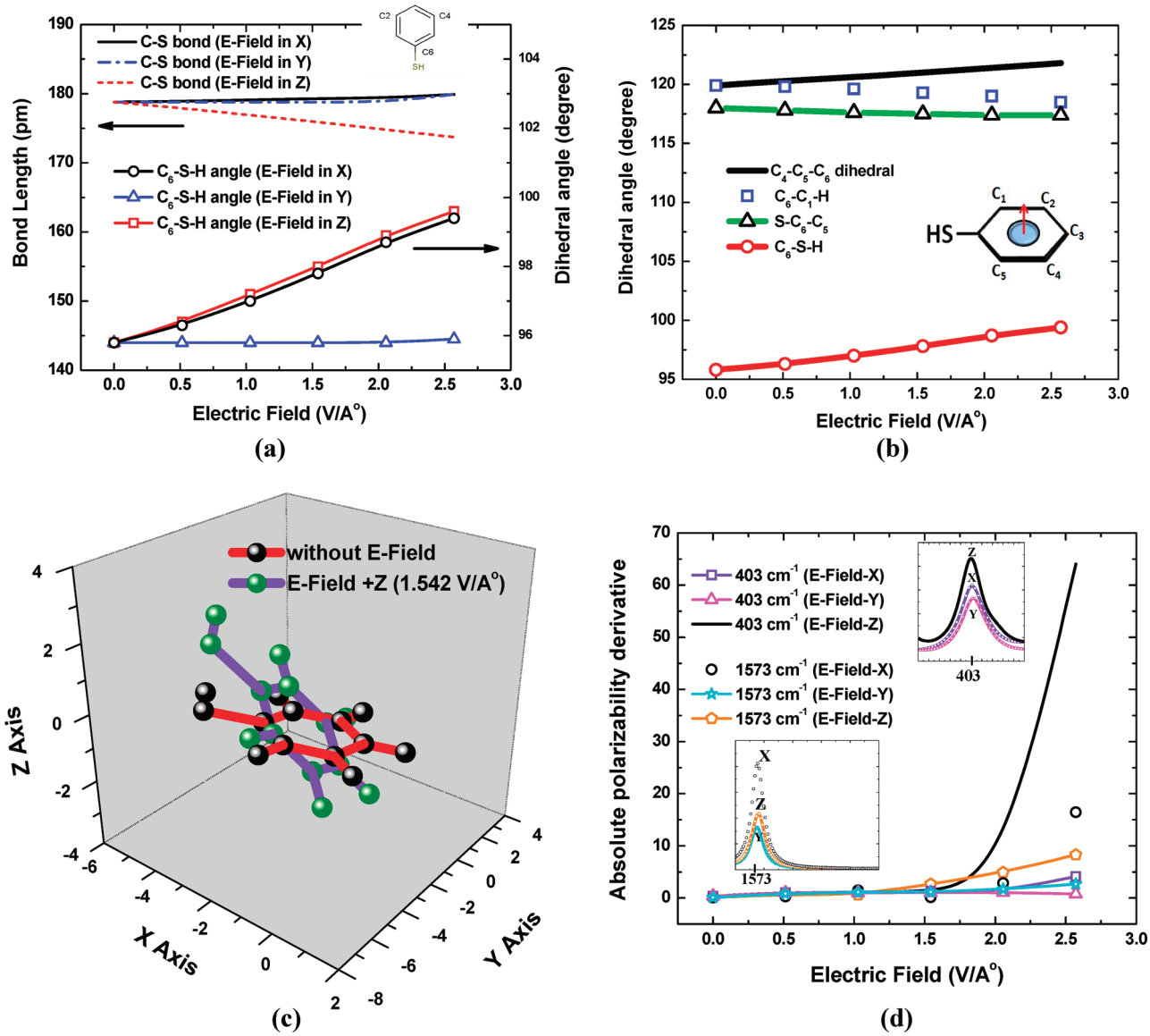

Figure 3. (a) Change in the C−S bond length and C−S−H dihedral angle as a function of electric field applied in the *X*, *Y*, and *Z* directions relative to the benzenethiol molecule. (b) Dihedral angle variation with built-in electric field perpendicular to the ring structure. (c) Change in orientation of the molecule due to application of electric field. (d) Absolute polarizability derivative (modulus of the polarizability derivative) at two Raman peaks (403 and 1573 cm^{-1}).

and there is a separate surface for each electronic configuration.[96] Figure 4 shows schematically that there must be an intermediate state created due to adsorption of benzenethiol to gold atoms as the excitation incident wave (532 nm or 2.33 eV) is far below the purely intramolecular electronic transitions level (4.1 eV), which is also supported by a recent theoretical model.[44] The increase in polarizability derivative (and subsequent enhanced Raman intensity) can be explained by the large change in the dipole moment due to a change in molecular conformation (and an increase in the bond length as shown in Figure 4) (please see the Supporting Information for more details). The increased dipole moment ($p = qd$) is depicted by a larger separation of two charges described by red and blue colors as observed for the HOMO level of benzenethiol. Since the polarizability of the molecule is related to the vibrational coordinates and the dipole moment, an increased in polarizability is expected. We also observed an increase in the absolute polarizability derivative (modulus of the polarizability derivative) along with increase in dipole moment (Figure 3d). The Raman scattering cross-section is proportional to the square of polarizability derivative $(d\sigma/d\Omega) \propto (d\alpha/dr)^2$.[97] Hence, an increase in Raman scattering cross-section is expected as a result of a large change in the polarizability derivative even in the absence of an electronic transition.

The metal−molecule Schottky barrier also induces the change of energy band gap of a benzenethiol molecule. As shown in Figure 5, the band gap of an isolated benzenethiol molecule is in the ultraviolet region, which makes the electronic level transition forbidden for visible excitations. The Fermi (HOMO) level of gold is somewhere in the middle of the molecule energy band gap. The energy difference between gold Fermi level and HOMO of an isolated molecule shows the viability of charge transfer scheme where charges can transfer from a metal atom cluster to the molecule or from the molecule to the metal cluster. Due to attaching gold atoms the density and number of accessible states in the hybrid system increase. In addition, the band gap shrinks due to the attachment of gold atoms that may make it possible to induce resonance Raman for visible excitations. It should be noted that the band gap of benzenethiol calculated in the present study is 4.092 eV, which is in close

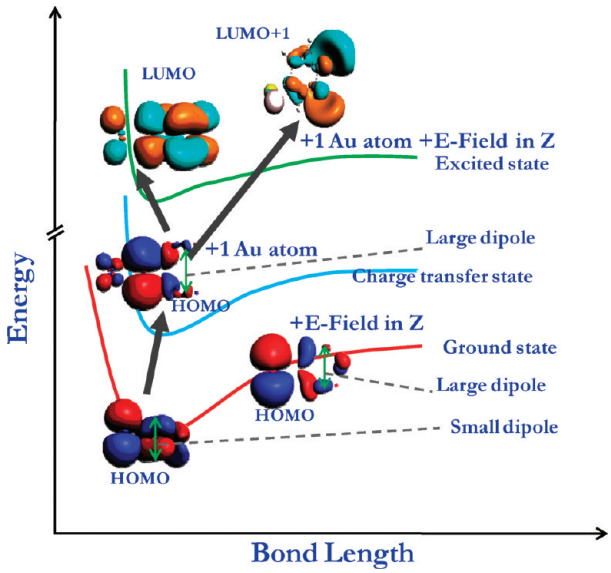

Figure 4. Sketch showing the schematic of the charge transfer scheme explained in terms of HOMO and LUMO states of the molecule. The enhancement in Raman scattering cross-section due to the large dipole moment change because of application of electric field, creation of an intermediate state due to attachment of the gold atom, and the combined effect of above two are shown.

agreement with the value of 4.027 eV calculated by Morton and Jensen.[34] Similarly, the band gap calculated in the present study for benzenethiol with three gold atoms configuration is 0.75 eV whereas for a similar system the value calculated by Letardi and Cleri[98] was 0.76 eV. The prediction of shrinking band gap due to adsorption is also in good agreement with the theoretical study by Saikin et al.[44] for benzenethiol adsorbed on a silver cluster. The built-in electric field further shrinks the band gap, increasing the probability of transition to higher excited states and further enlarging the Raman scattering cross-section.

The reason for shrinkage of the band gap (Figure 6a,b) due to adsorption to metal atoms can be described as follows. The ionic cores in the metal are assumed to give rise to a square potential well for the electrons and all states are filled up to the Fermi level, E_F.[71] The energy difference between E_F and the potential energy of an electron in the vacuum above this hypothetical surface, U_{vac}, is generally referred to as the *intrinsic* work function, Φ' (or chemical potential), of the metal (e.g., for gold it is 5.3 eV) (Figure 6c). However, because the potential well is not infinitely deep, there is always a finite probability of finding electrons outside the potential well; that is, electron density is "leaking out" from the metal into the vacuum.[99] Consequently, a dipole layer is formed with a positively charged region below the surface (red region) and negatively charged region (light blue) just outside the metal surface. This dipole layer is commonly referred to as the *surface dipole* and gives rise to a potential step across the metal surface (Figure 6d).[71] The surface dipole raises U_{vac} directly above the metal surface relative to E_F and leads to the *observed* work function, Φ, of the metal surface.[99]

Now when a benzenethiol molecule appears near the metal surface, there exists a mismatch of ionization potential (IP ∼ 8.32 eV)) of the molecule and the work function of metal (∼5.3 eV). As we pointed out earlier, this will lead to a Schottky barrier that will give rise to a built-in electric field directed from metal surface to the organic molecule. The developed electric field will oppose further leakage of electrons from the metal. So even for a weakly interacting (physisorbed or van der Waal interacting) species or for a strongly interacting (covalent bonded) species, the electron cloud leaking out of the metal surface is pushed back into the metal (Figure 6e).[100] This *push-back* (or *pillow*) effect always contributes to reduce the surface dipole and lower U_{vac} relative to E_F and, consequently, leads to a reduced work function, Φ_{mod}, of the sample.[71] The amount by which the surface dipole is reduced is generally known as the *interface dipole*.[71] The interface dipole is expected to lower the LUMO level of the organic molecule too. In the present study we have observed a reduction of ∼2.54 eV for the benzenethiol LUMO level. In addition, an interface dipole with its negative pole pointing toward the organic layer and its positive pole toward the metal is expected to increase the metal work function (i.e., decreases the Fermi energy) and increases the HOMO energy of the organic layer by adding an electrostatic energy;[101] as a result, the hole injection barrier (HIB) should be reduced (Figure 6b,e). In fact, in our simulation, we have observed an increase of 1.37 eV for the HOMO level of benzenethiol up on conjugation to gold, which reduces the HIB from 2.06 eV before conjugation to 0.69 eV after conjugation.

To elucidate the effect of magnitude of built-in electric field on Raman intensity, the Raman scattering spectra are simulated by calculating the Raman intensity as the function of applied electric field. Figure 7 shows that with application of a local built-in electric field of 1.028 V/Å (which is slightly lower than the theoretical electric field calculated earlier using simple model), one extra order of Raman enhancement was achieved in addition to the enhancement from the gold atom attachment. This shows that a built-in electric field can actually bridge the gap between high enhancement experimental observations and previous theoretical simulations. In fact, with an application of a high built-in field of 2.570 V/Å we achieved a 2−4 more orders of enhancement (please see Supporting Information), which points to the importance of a metal−molecular junction for the potential 10^{14} Raman enhancement.

Effect of Direction of Electric Field

The intensity of a vibrational mode is proportional to the square of scalar product of the electric field and the dipole moment derivative of the mode ($d\vec{\mu}/dQ$) as $I \propto |(d\vec{\mu}/dQ)\vec{E}|^2 = |(d\vec{\mu}/dQ)|^2|\vec{E}|^2 \cos^2\beta$,[102] where β is the angle between electric field, $\vec{E}$ and $d\vec{\mu}/dQ$. This shows that there is a strong dependence of Raman peak intensity to direction of the electric field. In fact, in our DFT simulation, we observed that applying the electric field in a direction parallel to the aromatic ring decreases the SERS enhancement, as shown in Figure 8. Further, aligning the electric field in gold−sulfur bond direction improved the signals. Finally, application of an electric field perpendicular to the aromatic ring further increases SERS enhancement. This concludes that molecular orientations relative to the built-in electric field in the junction dictate in this enhancement mechanism. The reorientation of a molecule relative to the surface due to changes in the electrode potential has been reported by Moskovits et al.[103] Subsequent detailed study using high resolution electron energy loss spectroscopy (HREELS) by Wan et al.[50] for benzenethiol adsorption to the Au (111) surface further confirms our hypothesis that molecular orientation relative to the built-in electric field plays an important role in the charge transfer mechanism in SERS.

Vibrational Shift in SERS

In general, all the Raman peak positions in SERS spectra are never consistent with those of the original Raman

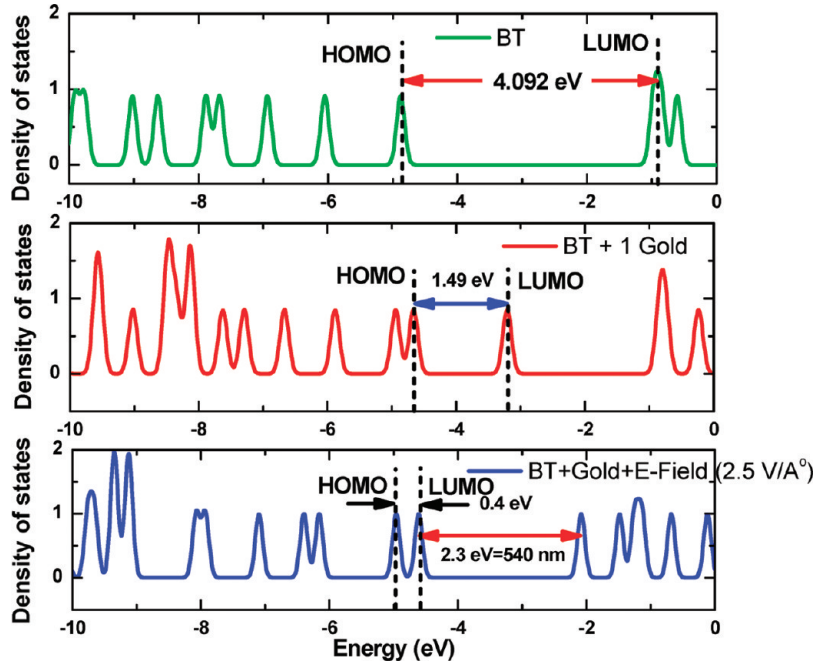

Figure 5. Density of state plot for isolated benzenethiol (BT), for the molecule adsorbed on one gold atom, and for when built-in electric field is applied to molecule adsorbed on the gold atom.

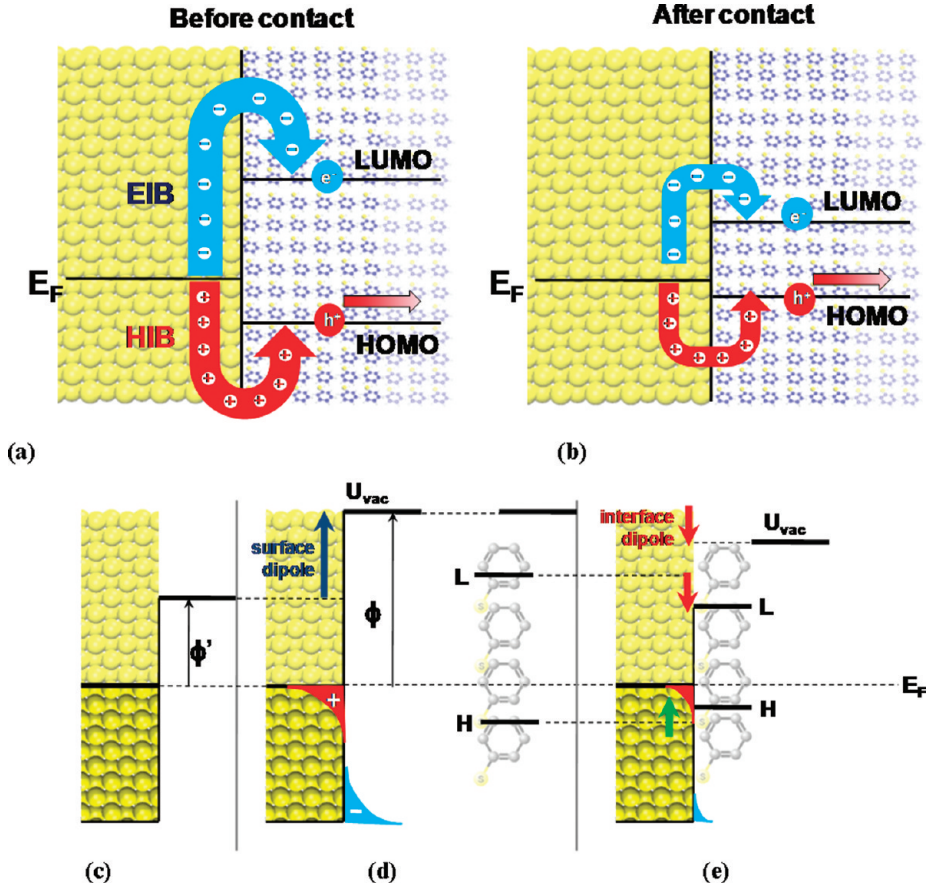

Figure 6. (a) Schematic energy-level diagram at a metal/organic molecule interface. (a) Position of the highest occupied molecular orbital (HOMO: H) and the lowest unoccupied molecular orbital (LUMO: L) of benzenethiol with respect to the Fermi level (E_F) of Au before contact. After contact (b), the HIB and EIB can be reduced. (c) Model of a metal surface (square potential well in the absence of a surface dipole. (d) As electrons leak out of the potential well forming surface dipole. (e) Upon interaction of the molecules, the electrons are pushed back into the metal, reducing the surface dipole and charge-carrier injection barriers.

spectra.[44,104−107] The frequency shifts of seven commonly observed modes in benzenethiol are compared to experimental SERS and DFT calculated data in Table 1. The values of the vibrational frequencies (termed as freq PhSH) are taken for neat benzenethiol from our experiments.[93] The vibrational band at $\omega_1 = 1005\ cm^{-1}$ is assigned to the ring breathing mode (β_{CCC})

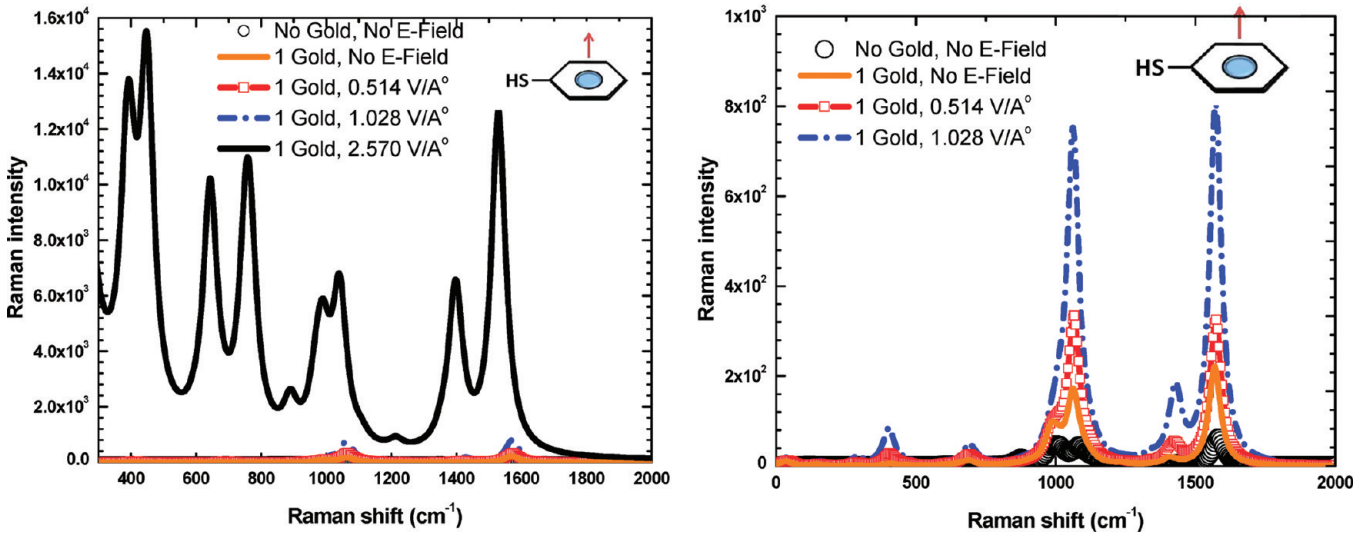

Figure 7. Enhancement due to the gold−benzenethiol Schottky barrier.

TABLE 1: Frequency Shifts of Benzenethiol Raman Active Vibrational Modes Due to Binding to the Metal and Application of Electric Field (in DFT)[a]

	ω_1	ω_2	ω_3	ω_4	ω_5	ω_6	ω_7
freq PhSH[93]	1005	1032	1099	1584	420	705	922
PhS-Ag (SERS)[93]	1006	1028	1078	1573	425	696	
PhSH-DFT	1002		1084	1584	403	691	875
PhSH-DFT (0.51)	991		1084	1580	403	696	882
PhSH-DFT (1.03)	992		1084	1578	403	691	882
PhSH-DFT (1.54)	989		1079	1570	400	676	882
PhSH-DFT (2.05)	981		1071	1564	426	631	869
PhSH-DFT (2.57)		1018	1047	1549	410	715	840
ref 105	1003	1027	1076	1576	422	695	
ref 106	1000	1025	1075	1575	420	695	
ref 107	1002	1026	1073	1573	420	693	
ref 44	1003	1024	1076	1574	419	697	907
PhS-Au_1 [present work]			1062	1560	403	693	
PhS-Au_1 (0.51)			1064	1571	408	693	
PhS-Au_1 (1.03)	988		1061	1573	409	693	
PhS-Au_1 (1.54)	983		1053	1563	409	693	
PhS-Au_1 (2.05)	979		1059	1551	382	712	
PhS-Au_1 (2.57)	1009	1035	1090	1571	408	713	922

[a] The frequencies are given in cm^{-1}. PhSH: benzenethiol. The numbers in parentheses are the electric field value in V/Å applied in DFT simulations.

(please see the Supporting Information for the movies), and the band at $\omega_2 = 1032$ cm^{-1} corresponds to a ring deformation mode (β_{CH}). The C−S stretching mode ($\beta_{CCC} + \upsilon_{CS}$), is given at $\omega_3 = 1099$ cm^{-1} while the computed Raman band at $\omega_4 = 1584$ cm^{-1} is associated with a totally symmetric ring stretching mode (υ_{CC}). The other important modes are $\omega_5 = 420$ ($\upsilon_{CS} + \beta_{CCC}$), $\omega_6 = 705$ ($\beta_{CCC} + \upsilon_{CS}$), and 922 cm^{-1} (β_{SH}). Note that the 922 cm^{-1} mode generally disappears in SERS spectra due to thiolate bond formation. The large shift in the C−S stretching mode (1099 cm^{-1}) in SERS can be attributed to the proximity effect as the vibrational mode is strongly enhanced by the interaction with the Au cluster.[44]

As described above, the C−C bond stretch mode on the aromatic ring was observed at 1584 cm^{-1} in the original Raman spectrum, which is consistent with our DFT simulation results. In a parallel SERS experiment reported in the paper,[93,107] the SERS peak for the same mode was observed at 1573 cm^{-1}. Apparently, the Raman peak position shifts in the SERS spectrum in comparison with the original Raman spectrum. Although with only one gold atom conjugation there is a shift of Raman peak position in our simulation from 1584 to 1560 cm^{-1}, it is not consistent with the experimental observation,

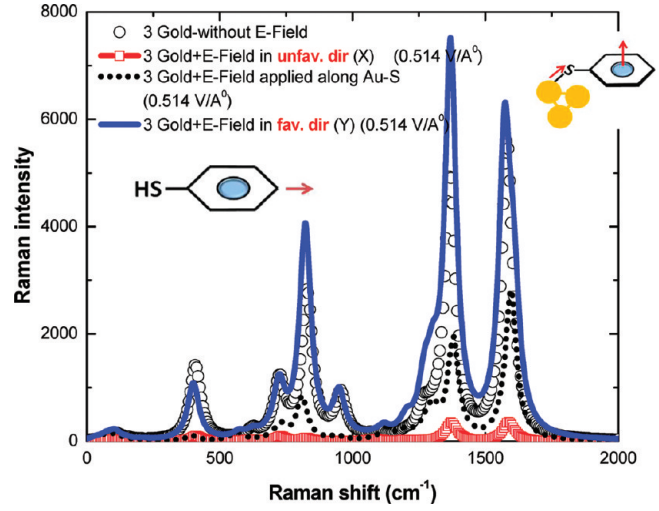

Figure 8. Effect of molecular orientation relative to the built-in electric field.

where it shifts to 1573 cm^{-1}. On the other hand, with including the built-in electric field effect (1.028 V/Å) in our DFT

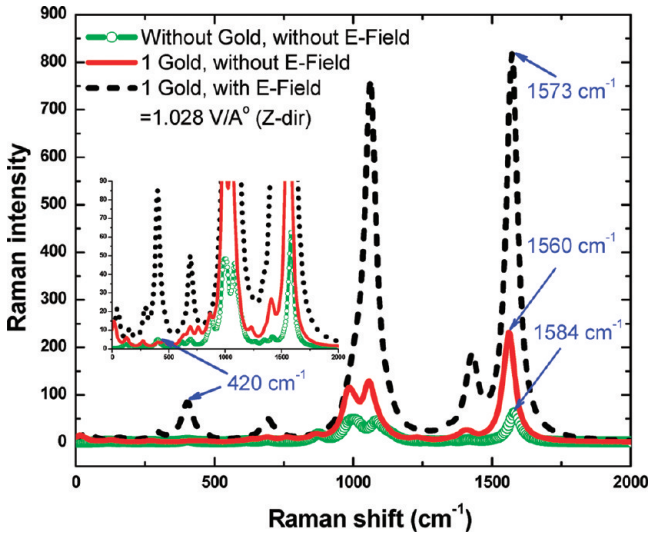

Figure 9. Explanation for the Raman peak shift. The inset shows the 420 cm^{-1} Raman peak position.

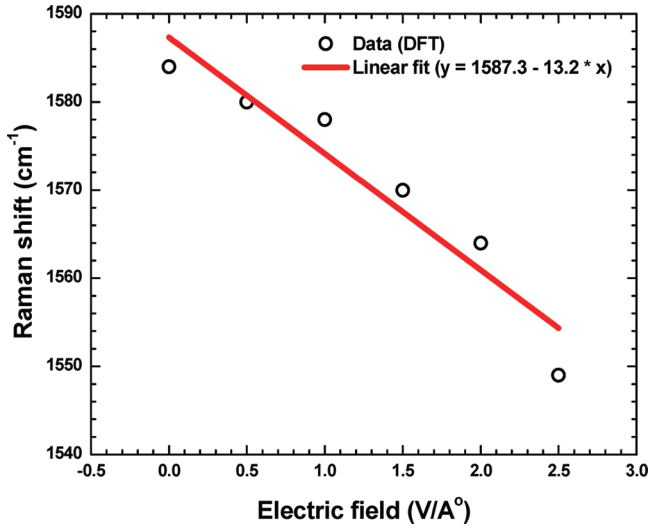

Figure 10. Effect of electric field on the Raman vibrational shift.

simulation we observed the SERS peak at 1573 cm^{-1}, which exactly matches with the experimental observation (Figure 9). Similarly, the large enhancement of the 420 cm^{-1} peak ($\beta_{CCC} + \upsilon_{CS}$), is obtained in our simulation only after taking into account of the metal molecular Schottky junction (Figure 9), which is also consistent with the experimental observations[93,107] and theoretical prediction.[44]

Finally, Figure 10 shows the vibrational shift observed in our DFT simulation when we an applied electric field of different magnitudes perpendicular to the ring structure. The plot is shown for a characteristic peak of 1573 cm^{-1} and corresponds to the case when the benzenethiol molecule is not attached to any gold atom (so this will discount any interference of charge transfer from the gold cluster and thus represents the effect purely due to electric field only). We observed a closely linear fall of vibrational shift of ring stretching mode (υ_{CC}) with electric field and the stark tuning rate was calculated to be 13.2 cm^{-1}/(V/Å). In fact, this value is very close to the vibrational shift observed (which ranges from ~10 to 13 cm^{-1}) in many SERS experiments for this particular characteristics peak.[105−107] In spite of not having enough statistics to prove our hypothesis, the results clearly points to a possible role of electric field of strength ~1 V/Å. In addition, though the accuracy and precision of DFT is in doubt,[108] still the correct trend of vibrational shift can be inferred from the present simulation. Since the inclusion of built-in electric field contribution leads to correct prediction of Raman peak shifts, we believe that the built-in electric field is playing an important role in SERS process.

Conclusion

In summary, we have performed a quantum mechanical simulation to study the effect of built-in electric field due to a Schottky barrier formed between the molecule monolayer and metallic SERS substrate. We found that the application of a built-in electric field changes the bond lengths and dihedral angles which lead to an alteration in the dipole moment. Further, this built-in field also causes a modification in the polarizability and polarizability derivatives of the molecule, which are mainly responsible for the drastic change in scattering cross-section observed in SERS. We have also shown that the order of enhancement that can be obtained in Raman scattering cross section is highly dependent on the direction of the built-in electric field. This helps to explain the nonrepeatability of many SERS experiments. Finally, adding a strong electrostatic built-in field can result in 2−4 more orders of enhancement in SERS for benzenethiol molecules.

Acknowledgment. This work is supported by Lawrence Livermore National Laboratory under Contract No. AC52-07NA27344. We thank Prof. Nick Fang, Mechanical Science and Engineering, University of Illinois, Urbana−Champaign, for the valuable discussions and suggestions. We also acknowledge support by the Defense Advanced Research Projects Agency (DARPA) and DARPA SERS S&T Fundamentals.

Supporting Information Available: Simulation results for dipole moments, polarizability, energy diagram, and electron density of benzenethiol molecules and additional results on simulated Raman spectra. Also included are the movies showing various vibrational modes in simulated Raman spectra. This material is available free of charge via the Internet at http://pubs.acs.org.

References and Notes

(1) Fleischmann, M.; Hendra, P. J.; McQuillan, A. J. Raman Spectra of Pyridine Adsorbed at a Silver Electrode. *Chem. Phys. Lett.* **1974**, *26*, 163–166.

(2) Jeanmaire, D. L.; Van Duyne, R. P. Surface Raman Spectroelectrochemistry: Part I. Heterocyclic, Aromatic, and Aliphatic Amines Adsorbed on the Anodized Silver Electrode. *J. Electroanal. Chem.* **1977**, *84*, 1–20.

(3) Albrecht, M. G.; Creighton, J. A. Anomalously Intense Raman Spectra of Pyridine at a Silver Electrode. *J. Am. Chem. Soc.* **1977**, *99*, 5217.

(4) Cotton, T. M.; Schultz, S. G.; Van Duyne, R. P. Surface-Enhanced Resonance Raman Scattering from Cytochrome c and Myoglobin Adsorbed on a Silver Electrode. *J. Am. Chem. Soc.* **1980**, *102*, 7962.

(5) Nie, S.; Emory, S. R. Probing Single Molecules and Single Nanoparticles by Surface-Enhanced Raman Scattering. *Science* **1997**, *275*, 1102–1106.

(6) Kneipp, K.; Wang, Y.; Kneipp, H.; Perelman, L. T.; Itzkan, I.; Dasari, R. R.; Feld, M. S. Single Molecule Detection using Surface-Enhanced Raman Scattering (SERS). *Phys. Rev. Lett.* **1997**, 78.

(7) Lyandres, O.; Shah, N. C.; Yonzon, C. R.; Walsh, J. T.; Glucksberg, M. R.; Van Duyne, R. P. Real-Time Glucose Sensing by Surface-Enhanced Raman Spectroscopy in Bovine Plasma Facilitated by a Mixed Decanethiol/Mercaptohexanol Partition Layer. *Anal. Chem.* **2005**, *77*, 6139.

(8) Lyandres, O.; Yuen, J. M.; Shah, N. C.; Van Duyne, R. P.; Walsh, J. J. T.; Glucksberg, M. R. Progress Toward an in Vivo Surface-Enhanced Raman Spectroscopy Glucose Sensor. *Diabetes technology therapeutics* **2008**, *10*, 257.

(9) Yonzon, C.; Lyandres, O.; Shah, N.; Dieringer, J.; Van Duyne, R Glucose Sensing with Surface-Enhanced Raman Spectroscopy. In *Surface-Enhanced Raman Scattering - Physics and Applications, Topics in Appl.*

Phys.; Kneipp, K., Moskovits, M., Kneipp, H., Eds.; Springer-Verlag: Berlin Heidelberg, 2006, 103, pp 367–379.

(10) Zamarion, V. M.; Timm, R. A.; Araki, K.; Toma, H. E. Ultrasensitive SERS Nanoprobes for Hazardous Metal Ions Based on Trimercaptotriazine-Modified Gold Nanoparticles. *Inorg. Chem.* **2008**, *47*, 2934.

(11) Zhang, X.; Shah, N. C.; Van Duyne, R. P. Sensitive and Selective chem/bio Sensing Based on Surface-Enhanced Raman Spectroscopy (SERS). *Vibr. Spectrosc.* **2006**, *42*, 2–8.

(12) Qian, X.; Peng, X.; Ansari, D. O.; Yin-Goen, Q.; Chen, G. Z.; Shin, D. M.; Yang, L.; Young, A. N.; Wang, M. D.; Nie, S. In Vivo Tumor Targeting and Spectroscopic Detection with Surface-Enhanced Raman Nanoparticle Tags. *Nat. Biotechnol.* **2008**, *26*, 90.

(13) Fujita, K.; Ishitobi, S.; Hamada, K.; Smith, N. I. Time-Resolved Observation of Surface-Enhanced Raman Scattering from Gold Nanoparticles during Transport through a Living Cell. *J. Biomed. Opt.* **2009**, *14*, 024038.

(14) Lombardi, J. R.; Birke, R. L. A Unified View of Surface-Enhanced Raman Scattering. *Acc. Chem. Res.* **2009**, *42*, 742.

(15) Moskovits, M. Surface Roughness and the Enhanced Intensity of Raman Scattering by Molecules Adsorbed on Metals. *J. Chem. Phys.* **1978**, *69*, 4159.

(16) Lombardi, J. R.; Birke, R. L.; Lu, T.; Xu, J. Charge-Transfer Theory of Surface Enhanced Raman Spectroscopy: Herzberg-Teller Contributions. *J. Chem. Phys.* **1986**, *84*, 4174.

(17) Lombardi, J. R.; Birke, R. L. A Unified Approach to Surface-Enhanced Raman Scattering. *J. Phys. Chem. C* **2008**, *112*, 5617.

(18) Campion, A.; Kambhampati, P. Surface-Enahnced Raman Scattering. *Chem. Soc. Rev.* **1998**, *27*, 241.

(19) Kneipp, K.; Kneipp, H.; Itzkan, I.; Dasari, R. R.; Feld, M. S. Surface-Enhanced Raman Scattering and Biophysics. *J. Phys. Condensed Matter* **2002**, *14*, R597.

(20) Furtak, T. E.; Macomber, S. H. Voltage-Induced Shifting of Charge-Transfer Excitations and their Role in Surface-Enhanced Raman Scattering. *Chem. Phys. Lett.* **1983**, *95*, 328–332.

(21) Pockrand, I.; Otto, A. Surface Enhanced and Disorder Induced Raman Scattering from Silver Films. *Solid State Commun.* **1981**, *37*, 109–112.

(22) Lombardi, J. R.; Birke, R. L.; Sanchez, L. A.; Bernard, I.; Sun, S. C. The Effect of Molecular Structure on Voltage Induced Shifts of Charge Transfer Excitation in Surface Enhanced Raman Scattering. *Chem. Phys. Lett.* **1984**, *104*, 240–247.

(23) Burstein, E.; Chen, Y. J.; Chen, C. Y.; Lundquist, S.; Tosatti, E. Giant" Raman Scattering by Adsorbed Molecules on Metal Surfaces. *Solid State Commun.* **1979**, *29*, 567–570.

(24) Persson, B. N. J. On the Theory of Surface-Enhanced Raman Scattering. *Chem. Phys. Lett.* **1981**, *82*, 561–565.

(25) Gersten, J. I.; Birke, R. L.; Lombardi, J. R. Theory of Enhanced Light Scattering from Molecules Adsorbed at the Metal-Solution Interface. *Phys. Rev. Lett.* **1979**, *43*, 147–150.

(26) Moskovits, M. Surface-Enhanced Spectroscopy. *Rev. Mod. Phys.* **1985**, *57*, 783.

(27) Otto, A.; Mrozek, I.; Grabhorn, H.; Akemann, W. Surface-Enhanced Raman Scattering. *J. Phys.: Condensed Matter* **1992**, *4*, 1143.

(28) Jin, R. Nanoparticle Clusters Light Up in SERS. *Angew. Chem. (Int. Ed. Engl.)* **2010**, *49*, 2826–2829.

(29) Sun, M.; Li, Z.; Liu, Y.; Xu, H. Direct Visual Evidence for Chemical Mechanisms of SERRS Via Charge Transfer in Au20-Pyrazine-Au20 Junction. *J. Raman Spectrosc.* **2009**, *40*, 1942.

(30) Xu, H. X.; Bjerneld, E. J.; Käll, M.; Börjesson, L. Spectroscopy of Single Hemoglobin Molecules by Surface Enhanced Raman Scattering. *Phys. Rev. Lett.* **1999**, 83.

(31) General Discussion. *Faraday Discuss.* **2006**, *132*, 227−247.

(32) Lazorenko-Manevich, R. M. Adatom Hypothesis as a Predominant Mechanism of Surface Enhanced Raman Scattering: A Review of Experimental Argumentation. *Russ. J. Electrochem.* **2005**, *41*, 799.

(33) Otto, A.; Timper, J.; Billmann, J.; Kovacs, G.; Pockrand, I. Surface Roughness Induced Electronic Raman Scattering. *Surf. Sci.* **1980**, *92*, L55.

(34) Morton, S. M.; Jensen, L. Understanding the Molecule-Surface Chemical Coupling in SERS. *J. Am. Chem. Soc.* **2009**, *131*, 4098.

(35) Udagawa, M.; Chou, C.; Hemminger, J. C.; Ushioda, S. Raman Scattering Cross Section of Adsorbed Pyridine Molecules on a Smooth Silver Surface. *Phys. Rev. B* **1981**, 23.

(36) Jiang, X.; Campion, A. Chemical Effects in Surface-Enhanced Raman Scattering: Pyridine Chemisorbed on Silver Adatoms on Rh (100). *Chem. Phys. Lett.* **1987**, *140*, 95–100.

(37) Zhao, L. L.; Jensen, L.; Schatz, G. C. Surface-Enhanced Raman Scattering of Pyrazine at the Junction between Two Ag_{20} Nanoclusters. *J. Am. Chem. Soc.* **2006**, *6*, 1234.

(38) Nikoobakht, B.; Wang, J.; El-Sayed, M. A. Surface-Enhanced Raman Scattering of Molecules Adsorbed on Gold Nanorods: Off-Surface Plasmon Resonance Condition. *Chem. Phys. Lett.* **2002**, *366*, 17–23.

(39) Fromm, D. P.; Sundaramurthy, A.; Kinkhabwala, A.; Schuck, P. J.; Kino, G. S.; Moerne, W. E. Exploring the Chemical Enhancement for Surface-Enhanced Raman Scattering with Au Bowtie Nanoantennas. *J. Chem. Phys.* **2006**, *124*, 061101.

(40) Peyser-Capadona, L.; Zheng, J.; Gonzalez, J. I.; Lee, T. H.; Patel, S. A.; Dickson, R. M. Nanoparticle-Free Single Molecule Anti-Stokes Raman Spectroscopy. *Phys. Rev. Lett.* **2005**, *94*, 058301.

(41) Zheng, J.; Ding, Y.; Tian, B.; Wang, Z. L.; Zhuang, X. Luminescent and Raman Active Silver Nanoparticles with Polycrystalline Structure. *J. Am. Chem. Soc.* **2008**, *130*, 10473.

(42) Yang, L.; Jiang, X.; Ruan, W.; Zhao, B.; Xu, W.; Lombardi, J. R. Observation of Enhanced Raman Scattering for Molecules Adsorbed on TiO_2 Nanoparticles: Charge-Transfer Contribution. *J. Phys. Chem. C* **2008**, *112*, 20098.

(43) Jensen, L.; Aikens, C. M.; Schatz, G. C. Electronic Structure Methods for Studying Surface-Enhanced Raman Scattering. *Chem. Soc. Rev.* **2008**, *37*, 1061.

(44) Saikin, S. K.; Olivares-Amaya, R.; Rappoport, D.; Stopa, M.; Aspuru-Guzik, A. On the Chemical Bonding Effects in the Raman Response: Benzenethiol Adsorbed on Silver Clusters. *Phys. Chem. Chem. Phys.* **2009**, *11*, 9401.

(45) Otto, A. The Chemical (Electronic) Contribution to Surface-Enhanced Raman Scattering. *J. Raman Spectrosc.* **2005**, *36*, 497.

(46) Aroca, R. F.; Clavijo, R. E.; Halls, M. D.; Schlegel, H. B. Surface-Enhanced Raman Spectra of Phthalimide. Interpretation of the SERS Spectra of the Surface Complex Formed on Silver Islands and Colloids. *J. Phys. Chem. A* **2000**, *104*, 9505.

(47) Jensen, L.; Zhao, L. L.; Autschbach, J.; Schatz, G. C. Theory and Method for Calculating Resonance Raman Scattering from Resonance Polarizability Derivatives. *J. Chem. Phys.* **2005**, *123*, 174110.

(48) Jensen, L.; Zhao, L. L.; Schatz, G. C. Size-Dependence of the Enhanced Raman Scattering of Pyridine Adsorbed on Ag_n (n = 2−8, 20) Clusters. *J. Phys. Chem. C* **2007**, *111*, 4756.

(49) Nara, J.; Higai, S.; Morikawa, Y.; Ohno, T. Density Functional Theory Investigation of Benzenethiol Adsorption on Au (111). *J. Chem. Phys.* **2004**, *120*, 6705.

(50) Wan, L.; Terashima, M.; Noda, H.; Osawa, M. Molecular Orientation and Ordered Structure of Benzenethiol Adsorbed on Gold (111). *J. Phys. Chem. B* **2000**, *104*, 3569.

(51) Vivoni, A.; Birke, R. L.; Foucault, R.; Lombardi, J. R. Ab Initio Frequency Calculations of Pyridine Adsorbed on an Adatom Model of a SERS Active Site of a Silver Surface. *J. Phys. Chem. B* **2003**, *107*, 5557.

(52) Wu, D. Y.; Duan, S.; Ren, B.; Tian, Z. Q. Density Functional Theory Study of Surface-Enhanced Raman Scattering Spectra of Pyridine Adsorbed on Noble and Transition Metal Surfaces. *J. Raman Spectrosc.* **2005**, *36*, 533.

(53) Cardini, G.; Miranda, M. M. Density Functional Study on the Adsorption of Pyrazole Onto Silver Colloidal Particles. *J. Phys. Chem. B* **2002**, *106*, 6875.

(54) Wu, D. Y.; Ren, B.; Jiang, Y. X.; Xu, X.; Tian, Z. Q. Density Functional Study and Normal-Mode Analysis of the Bindings and Vibrational Frequency Shifts of the Pyridine-M (M) Cu, Ag, Au, Cu+, Ag+, Au+, and Pt) Complexes. *J. Phys. Chem. A* **2002**, *106*, 9042.

(55) Cardini, G.; Muniz-Miranda, M.; Pagliai, M.; Schettino, V. A Density Functional Study of the SERS Spectra of Pyridine Adsorbed on Silver Clusters. *Theor. Chem. Acc.* **2007**, *117*, 458.

(56) Johansson, P. Illustrative Direct Ab Initio Calculations of Surface Raman Spectra. *Phys. Chem. Chem. Phys.* **2005**, *7*, 475.

(57) Wu, D. Y.; Hayashi, M.; Lin, S. H.; Tian, Z. Q. Theoretical Differential Raman Scattering Cross-Sections of Totally-Symmetric Vibrational Modes of Free Pyridine and pyridine-metal Cluster Complexes. *Spectrochim. Acta Part A: Mol. Biomol. Spectrosc.* **2004**, *60*, 137–146.

(58) Lambert, D. K. Vibrational Stark Effect of Adsorbates at Electrochemical Interfaces. *Electrochim. Acta* **1996**, *41*, 623–630.

(59) Lambert, D. K. Electric Field Induced Change of Adsorbate Vibrational Line Strength. *J. Chem. Phys.* **1991**, *94*, 6237.

(60) Nart, F. C.; Iwasita, T. Static Field Effect on the Band Intensity of Adsorbed Sulfate Ions. *Electrochim. Acta* **1996**, *41*, 631–636.

(61) Pomfret, M. B.; Pietron, J. J.; Owrutsky, J. C. Measurement of Benzenethiol Adsorption to Nanostructured Pt, Pd, and PtPd Films using Raman Spectroelectrochemistry. *Langmuir* **2010**, *26*, 6809.

(62) Gomez, R.; Perez, J. M.; Gullon, J. S.; Montiel, V.; Aldaz, A. In Situ Surface Enhanced Raman Spectroscopy on Electrodes with Platinum and Palladium Nanoparticle Ensembles. *J. Phys. Chem. B* **2004**, *108*, 9943.

(63) Sawai, Y.; Takimoto, B.; Nabika, H.; Ajito, K.; Murakoshi, K. Control of Near-Infrared Optical Response of Metal Nano-Structured Film on Glass Substrate for Intense Raman Scattering. *Faraday Discuss.* **2006**, *132*, 179.

(64) Kilitziraki, M.; Moore, A. J.; Petty, M. C.; Bryce, M. R. Evaporated Thin Films of Tetrathiafulvalene Derivatives and their Charge-Transfer Complexes. *Thin Solid Films* **1998**, *335*, 209–213.

(65) Geiser, U. *Toward crystal design in organic conductors and superconductors; 1999, Proceedings of the 28th International School of Crystallography*, Erice, Italy, May 1999.

(66) Horowitz, G. Organic Field-Effect Transistors. *Adv. Mater.* **1998**, *10*, 365.

(67) Kymissis, I. *Organic Field Effect Transistors, Theory, Fabrication and Characterization*; Springer: Berlin, 2009; Chapter 2.

(68) Yamashita, Y. Organic Semiconductors for Organic Field-Effect Transistors. *Sci. Technol. Adv. Mater.* **2009**, *10*, 024313.

(69) Schottky, W. *Phs. Z* **1940**, *41*, 570.

(70) Bardeen, J. Surface States and Rectification at a Metal Semi-Conductor Contact. *Phys. Rev.* **1947**, *71*, 717.

(71) Heimel, G.; Romaner, L.; Zojer, E.; Bredas, J. The Interface Energetics of Self-Assembled Monolayers on Metals. *Acc. Chem. Res.* **2008**, *41*, 729.

(72) Heimel, G.; Romaner, L.; Brédas, J.; Zojer, E. Organic/metal Interfaces in Self-Assembled Monolayers of Conjugated Thiols: A First-Principles Benchmark Study. *Surf. Sci.* **2006**, *600*, 4548–4562.

(73) Heimel, G.; Romaner, L.; Bredas, J.; Zojer, E. Interface Energetics and Level Alignment at Covalent Metal-Molecule Junctions: π-Conjugated Thiols on Gold. *Phys. Rev. Lett.* **2006**, *96*, 196806.

(74) Ishii, H.; Sugiyama, K.; Ito, E.; Seki, K. Energy Level Alignment and Interfacial Electronic Structures at organic/metal and organic/organic Interfaces. *Adv. Mater.* **1999**, *11*, 605.

(75) Campbell, I. H.; Davids, P. S.; Smith, D. L.; Barashkov, N. N.; Ferraris, J. P. The Schottky Energy Barrier Dependence of Charge Injection in Organic Light-Emitting Diodes. *Appl. Phys. Lett.* **1998**, *72*, 1863.

(76) Betti, M. G.; Kanjilal, A.; Mariani, C.; Vazquez, H.; Dappe, Y. J.; Ortega, J.; Flores, F. Barrier Formation at Organic Interfaces in a Cu (100)-Benzenethiolate-Pentacene Heterostructure. *Phys. Rev. Lett.* **2008**, *100*, 027601.

(77) de Boer, B.; Hadipour, A.; Mandoc, M. M.; van Woudenbergh, T.; Blom, P. W. M. Tuning of Metal Work Functions with Self-Assembled Monolayers. *Adv. Mater.* **2005**, *17*, 621.

(78) Chen, J.; Reed, M. A.; Rawlett, A. M.; Tour, J. M. Large on-Off Ratios and Negative Differential. *Science* **1999**, *286*, 1550.

(79) Whelan, C. M.; Smyth, M. R.; Barnes, C. J. HREELS, XPS, and Electrochemical Study of Benzenethiol Adsorption on Au(111). *Langmuir* **1999**, *15*, 126.

(80) Pauling, L. The Nature of the Chemical Bond. Application of Results obtained from the Quantum Mechanics and from a Theory of Paramagnetic Susceptibility to the Structure of Molecules. *J. Am. Chem. Soc.* **1931**, *53*, 1367. Also in: Pauling, L. *The nature of the Chemical Bond*, 3rd ed.; Cornell University Press: New York, 1960.

(81) Valiskó, M.; Boda, D. Relative Permittivity of Polar Liquids. Comparison of Theory, Experiment, and Simulation. *J. Phys. Chem. B* **2005**, *109*, 6355.

(82) Peisert, H.; Knupfer, M.; Fink, J. Energy Level Alignment at organic/metal Interfaces: Dipole and Ionization Potential. *Appl. Phys. Lett.* **2002**, *81*, 2400.

(83) Nam, P. C.; Nguyen, M. T.; Chandra, A. K. Theoretical Study of the Substituent Effects on the S−H Bond Dissociation Energy and Ionization Energy of 3-Pyridinethiol: Prediction of Novel Antioxidant. *J. Phys. Chem. A* **2006**, *110*, 10911.

(84) Ionization potential of Benzenethiol. http://www.bis.fm/assets/documents/faxdatasheets/Ion%20Science%20PhoCheck+2000%2010.6eV%20Gas%20Detection%20Table.pdf (accessed 07/09, 2010).

(85) Sze, S. M. In *Physics of Semiconductor Devices*, 2nd ed.; John Wiley Sons, Inc.: Hoboken, NJ, 2007.

(86) Yokota, K.; Taniguchi, M.; Kawai, T. Metal-Molecule Interfaces Formed by Noble-Metal-Chalcogen Bonds for Nanoscale Molecular Devices. *J. Phys. Chem. C* **2010**, *114*, 4050.

(87) Braun, S.; Salaneck, W. R.; Fahlman, M. Energy-Level Alignment at organic/metal and organic/organic Interfaces. *Adv. Mater.* **2009**, *21*, 1450.

(88) Tian, W.; Datta, S.; Hong, S.; Reifenberger, R.; Henderson, J. I.; Kubiak, C. P. Conductance Spectra of Molecular Wires. *J. Chem. Phys.* **1998**, *109*, 2874.

(89) ADF: Amsterdam Density Functional software. http://www.scm.com.

(90) Velde, Te. G.; Bickelhaupt, F. M.; Baerends, E. J.; Guerra, C. F.; Van Gisbergen, S. J. A.; Snijders, J. G.; Ziegler, T. Chemistry with ADF. *J. Comput. Chem.* **2001**, *22*, 931.

(91) Becke, A. D. Density-Functional Exchange-Energy Approximation with Correct Asymptotic Behavior. *Phys. Rev. A, At., Mol., Opt. Phys.* **1988**, *38*, 3098.

(92) Perdew, J. P. Density-Functional Approximation for the Correlation Energy of the Inhomogeneous Electron Gas. *Phys. Rev. B* **1986**, 33.

(93) Gartia, M. R.; Xu, Z.; Behymer, E.; Nguyen, H.; Britten, J. A.; Larson, C.; Miles, R.; Bora, M.; Chang, A. S. P.; Bond, T. C.; Liu, G. L. Rigorous Surface Enhanced Raman Spectral Characterization of Large-Area Ultrahigh-Uniformity Silver-Coated Tapered Silica Nanopillar Arrays. *Nanotechnology* **2010**, *21*, 395701.

(94) Etchegoin, P. G.; Galloway, C.; Le Ru, E. C. Polarization-Dependent Effects in Surface-Enhanced Raman Scattering (SERS). *Phys. Chem. Chem. Phys.* **2006**, *8*, 2624.

(95) Arenas, J. F.; Woolley, M. S.; Otero, J. C.; Marcos, J. I. Charge Transfer Processes in Surface-Enhanced Raman Scattering. Franck-Condon Active Vibrations of Pyridine. *J. Phys. Chem.* **1996**, *100*, 3206.

(96) Garraway, B.; Stenholm, S.; Suominen, K. A. Adventures in Wave Packet Land. *Phys. World* **1993**, 46.

(97) van Gisbergen, S. J. A.; Snijders, J. G.; Baerends, E. J. Application of Time-Dependent Density Functional Response Theory to Raman Scattering. *Chem. Phys. Lett.* **1996**, *259*, 599–604.

(98) Letardi, S.; Cleri, F. Interaction of Benzene Thiol and Thiolate with Small Gold Clusters. *J. Chem. Phys.* **2004**, *120*, 10062.

(99) Lang, N. D.; Kohn, W. Theory of Metal Surfaces: Work Function. *Phys. Rev. B* **1971**, 3.

(100) Witte, G.; Lukas, S.; Bagus, P. S.; Woll, C. Vacuum Level Alignment at organic/metal Junctions: "Cushion" Effect and the Interface Dipole. *Appl. Phys. Lett.* **2005**, *87*, 263502.

(101) Crispin, X.; Geskin, V.; Crispin, A.; Cornil, J.; Lazzaroni, R.; Salaneck, W. R.; Bredas, J. L. Characterization of the Interface Dipole at Organic/Metal Interfaces. *J. Am. Chem. Soc.* **2002**, *124*, 8141.

(102) Allara, D. L.; Nuzzo, R. G. Spontaneously Organized Molecular Assemblies. 2. Quantitative Infrared Spectroscopic Determination of Equilibrium Structures of Solution-Adsorbed n -Alkanoic Acids on an Oxidized Aluminum Surface. *Langmuir* **1985**, *1*, 66.

(103) Moskovits, M.; DiLella, D. P.; Maynard, K. J. Surface Raman Spectroscopy of a Number of Cyclic and Molecular Reorientation Aromatic Molecules Adsorbed on Silver: Selection Rules and Molecular Reorientation. *Langmuir* **1988**, *4*, 76.

(104) Joo, T. H.; Kim, M. S.; Kim, K. Surface-Enhanced Raman Scattering of Benzenethiol in Silver Sol. *J. Raman Spectrosc.* **1987**, *18*, 57.

(105) Biggs, K. B.; Camden, J. P.; Anker, J. N.; Van Duyne, R. P. Surface-Enhanced Raman Spectroscopy of Benzenethiol Adsorbed from the Gas Phase Onto Silver Film Over Nanosphere Surfaces: Determination of the Sticking Probability and Detection Limit Time. *J. Phys. Chem. A* **2009**, *113*, 4581.

(106) Carron, K. T.; Hurley, L. G. Axial and Azimuthal Angle Determination with Surface-Enhanced Raman Spectroscopy: Thiophenol on Copper, Silver, and Gold Metal Surfaces. *J. Phys. Chem.* **1991**, *95*, 9979.

(107) Aggarwal, R. L.; Farrar, L. W.; Diebold, E. D.; Polla, D. L. Measurement of the Absolute Raman Scattering Cross Section of the 1584-cm^{-1} Band of Benzenethiol and the Surface-Enhanced Raman Scattering Cross Section Enhancement Factor for Femtosecond Laser-Nanostructured Substrates. *J. Raman Spectrosc.* **2009**, *40*, 1331.

(108) Cohen, A. J.; Sánchez, P. M.; Yang, W. Insights into Current Limitations of Density Functional Theory. *Science* **2008**, *321*, 792.

JP1065083